Light-induced 3D-printing of DNA-based Responsive Hydrogels

Additive Manufacturing 124 (2026) 105231

Contents lists available at ScienceDirect

Additive Manufacturing

journal homepage: www.elsevier.com/locate/addma

Light-induced 3D-printing of DNA-based responsive hydrogels

Cristiana Drago [a,b], Désirée Baruffaldi [a,b], Candido Fabrizio Pirri [a,b,c], Ignazio Roppolo [a,b,c,*], Francesca Frascella [a,b]

[a] Department of Applied Science and Technology (DISAT), Politecnico di Torino, Corso Duca degli Abruzzi 24, Turin 10129, Italy
[b] PoliTOBioMEDLab, Politecnico di Torino, Corso Duca degli Abruzzi 24, Turin 10129, Italy
[c] Center for Sustainable Future Technologies, Italian Institute of Technology, Via Livorno 60, Turin 10144, Italy

ARTICLE INFO

Keywords:
Vat 3d printing
Smart hydrogels
DNA technologies
Stimuli responsive
Hybridization chain reaction

ABSTRACT

DNA-responsive hydrogels are a powerful class of materials with programmable functionalities, and have attracted growing interest in the last decade. This work introduces a fabrication strategy based on vat 3D printing Digital Light Processing (DLP) to create hybrid hydrogel architectures incorporating acrydite-modified DNA as a co-monomers. The test performed demonstrates that the molecular integrity of the DNA strands is preserved in the 3D printing process, enabling a specific and selective volumetric expansion triggered by the hybridization chain reaction (HCR) of complementary hairpins. By optimizing the printing parameters, well-defined complex 3D objects and multi-material structures are fabricated using minimal resin volumes (less than 100 μL). The hydrogel properties are also validated through reversible dehybridization cycles. Moreover, these materials show the ability to retain molecular recognition even in complex genomic environments, demonstrating the selectivity of the fabricated structures. These results establish a synergistic platform where advanced 3D design and molecular-scale responsiveness converge, opening new perspectives for the realization of sophisticated stimulus-responsive devices and advanced sensing applications.

1. New concepts

Deoxyribonucleic acid (DNA) -based hydrogels represent forefront research in contemporary materials science, as they can be considered as semi-living materials, in which inert synthetic polymers coexist with DNA macromolecules, that can modulate their shape and dimension in response to environmental stimuli. Moreover, DNA enables programmable and controlled reactions, taht can be exploited in several fields such as biomedicine and sensors, owing to its highly specific and modular structure. Pioneering investigations in this field showed the feasibility of fabricating these materials; however, these were limited to flat, bidimensional specimens. In this study, for the first time DNA-based materials are fabricated via vat photopolymerization 3D printing technology to allow the production of complex 3-dimensional DNA based hydrogels, without compromising the properties of the materials. This achievement represents a step forward for this class of materials, which can open to their use in new applications (e.g. advanced recognition), including the possibility to fabricate multimaterials, in which reactive species are confined in well-defined portions of the device.

2. Introduction

Hydrogels, i.e. materials able to contain a high amount of water, are gaining importance in the last decades, in particular for their applications in biomedical field, soft sensing and robotics [1]. Among them, the so called smart hydrogels have attracted increasing interest, since their dynamic behavior can be exploited for advanced applications [2,3]. Smart hydrogels encompass many different properties, such as the responsiveness to external triggers, the tunability of mechanical properties and the self-healing [4]. Such properties are provided by the chemical composition of their polymeric network, that can be designed to respond to targeted stimuli such as temperature, pH, light or target organic molecules [3,5].

Among the latter, deoxyribonucleic acid (DNA) is as an excellent candidate for the nanoscale construction of soft materials, emerging as functional polymer beyond its traditional role in biomedicine [6,7]. In 1996, for the first time DNA oligonucleotides were integrated into a hydrogel based on a synthetic polymeric network [8]. Thereafter, DNA-based hydrogels have been developed for the advancement of personalized medicine, targeted therapies, sophisticated diagnostic

* Corresponding author at: Department of Applied Science and Technology (DISAT), Politecnico di Torino, Corso Duca degli Abruzzi 24, Turin 10129, Italy
E-mail address: ignazio.roppolo@polito.it (I. Roppolo).

https://doi.org/10.1016/j.addma.2026.105231
Received 17 December 2025; Received in revised form 29 April 2026; Accepted 5 May 2026
Available online 7 May 2026

systems and soft-robotics [9–12].

The success of DNA-based hydrogels can be attributed to the versatile and modular nature of this biomolecule. The sequence of nitrogenous bases within a DNA strand can be programmed in a highly specific and precise manner. This allows for sequence-dictated three-dimensional organizations and for highly specific supramolecular interactions with complementary sequences. Furthermore, previous studies have reported the ability of DNA oligonucleotides to respond to a wide range of stimuli [11]. This behavior can be either sequence-dictated - e.g. 3D structural variation of oligonucleotides driven by changes in pH conditions - [13] or aspecific - e.g. DNA responsiveness to temperature [14]. Another promising strategy is the functionalization of DNA molecules to provide additional tailored responses to external stimuli. For instance, when responsiveness to light is sought, azobenzene or small molecules with acrylic groups can be included within the backbone of the DNA strands [15,16].

Additionally, the exploitation of the characteristics of DNA-based hydrogels can be enabled by selected fabrication methods. Light-based technologies are a benchmark in this context, because those can be employed to fabricate hydrogels when fine customization of the material properties and high spatial resolution are required [17]. In fact, light can activate spatially controlled chemical reactions, allowing localized polymerization that can be used in different technologies to scale fabrication down to the micro- and nanoscale. Pioneering recent works have showed the possibility to employ photolithography to fabricate DNA-based structures with controllable response [16,18–20]. In these studies, Gracias and Schulman's group presented innovative strategies to fabricate hybrid DNA-based hydrogels. Then, according to the materials design and contour conditions, those structures could swell, shrink and move in response to precise DNA sequences [16,18,19]. These straightforward results are however confined to 2D space, without exploring the possible opportunities of 3D parts.

Inspired by these cornerstone investigations, in this study the fabrication of DNA-responsive hydrogels was translated to the third dimension, by applying 3D printing technologies. Among all the available approaches, vat 3D printing, in particular digital light processing (DLP), is one of the most advantageous since it allows to reach high accuracy (in the order tens of microns) in a wide range of materials, improving production efficiency and allowing quicker customization of the desired tridimensional geometry [21]. Recently, the DLP technology has turned out to be a very effective in the hydrogels production, especially for biomedical applications, where fine customization of micropatterns is sought [22]. However, to the best of our knowledge, DNA-based hydrogels were never developed with this technology. The combination of these materials with this 3D printing technology allows to explore new strategies compared to standard photolithography. In the latter, the use of masks restrains 3D capabilities and requires an alignment system that can be expensive, time-consuming, and with limited scalability, especially in terms of designs. In contrast, DLP 3D printing offers a more streamlined process, enabling the rapid fabrication of complex geometries without the need for masks and support materials. Its layer-by-layer approach, combined with digital projection, ensures rapid and versatile customization, making it a valid alternative for DNA-based hydrogel fabrication. [23]

Summarizing, the aim of this work is to employ DLP 3D printing to produce functional DNA-based hydrogels. In general, the use of (meth) acrylates is widely recognized as a standard approach in light-based processes. This is due to their well-established reactivity in the presence of photogenerated radicals [23,24]. For this reason, short sequences of acrydite-modified DNA were added into a photocurable resin based on (meth)acrylate pre-polymers (Fig. 1.**a**). The acrydite-functionalization introduces a methacrylic group at the 5' moiety of the DNA strands, enabling them to covalently react with the other components of the resin during photopolymerization.

Previous works demonstrated that the mechanical properties are mainly related to the polymeric backbone of the hydrogel, while its

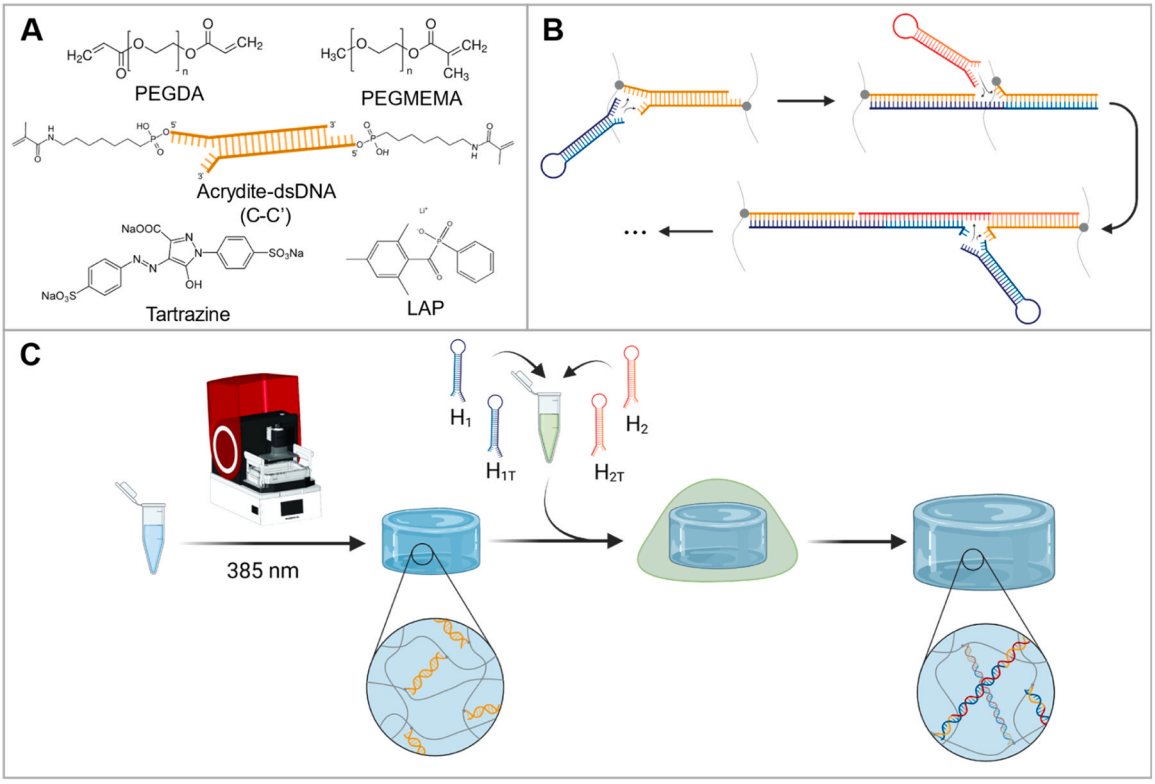

Fig. 1. a) Chemical structure of pre-polymers (PEGDA and PEGMEMA), acrydite-DNA, light absorber (tartrazine) and photoinitiator (LAP) in the photocurable resin. **b)** Schematic illustration of the implementation of DNA hairpins through HCR within the hydrogel. **c)** Process flow of the hydrogel expansion through hybridization chain reaction (HCR).

responsiveness can be associated to the DNA molecules [16,18,19]. Here, we triggered hydrogels through the hybridization chain reaction (HCR) process. This approach involves the addition of nucleic acid fuel, specifically single-stranded DNA molecules designed in a hairpin structure capable of opening upon interaction with target sequences. So, when the hydrogel is immersed in a proper buffer containing complementary hairpins (H1, $H1_T$, H2 and $H2_T$ in Fig. 1), the hairpins sequentially hybridize with the DNA molecules into the hydrogel (C and C'), as shown in Fig. 1.b [25,26]. This interaction at the microscale leads to the incorporation of additional DNA strands, inducing structural changes within the hydrogel network. As a result, the hydrogel undergoes a controlled volumetric expansion, which becomes evident at the macroscale (Fig. 1.c) [16,18].

3. Results and discussion

The choice of the ingredients for preparing the 3D printable photocurable formulations has initially been inspired by Gracias *et al.*'s work, as reference for selecting the specific DNA sequences promoting HCR (Table S1, Supporting Information) [18]. However, formulations needed adjustments to be suitable for light induced 3D printing.

Acrydite-DNA strands (C and C') must hybridize before the inclusion into resin, to act as initiator points for the HCR process. To achieve this, a thermal cycle on a solution containing both types of sequences has been performed (see Experimental section). Then, an electrophoretic run was conducted to verify the effectiveness of the process (Figure S1.a, Supporting Information).

With regard to the polymeric network, poly(ethylene)glycol diacrylate (PEGDA) with a molecular weight of 700 Da (PEGDA 700) was initially selected for developing the photocurable formulations, since it is commonly adopted in DLP 3D printing for its cost-effectiveness, compatibility with biological materials and the ability for enabling fast printing processes [27,28]. The choice of the photo-initiator, instead, derived from preliminary studies on their absorbance spectrum and on their influence on the mechanical properties of the hydrogel (Figure S2, Supporting Information). From these, we identified lithium phenyl-2,4,6 trimethylbenzoylphosphinate (LAP) as the most appropriate. Despite the good printability achieved with this PEGDA-based formulation (Table S2), the DNA-driven expansion was not statistically consistent (Figure S3, Supporting Information). This can be related to the high crosslinking density of the PEGDA 700 hydrogel networks, which limits the swelling and the DNA driven expansion. To overcome this issue and to obtain a looser network, a monofunctional monomer, poly(ethylene glycol)methyl ether methacrylate with molecular weight of 950 Da (PEGMEMA 950), was added to the photocurable resin. This monomer was selected since it is water soluble without bearing groups that can form H-bonds, to avoid possible interaction with DNA. Previous works have also shown that the addition of PEGMEMA to PEGDA-based resins influences polymerization kinetics and the hydrogel mechanical properties [29]. For this reason, photorheological tests have been performed on formulations containing different proportions of the two (meth)acrylates (Figure S4, Supporting Information). They revealed that the formulation with a 2:1 molar ratio of PEGDA to PEGMEMA was a suitable trade-off between mechanical properties and reactivity, while resins with higher content of PEGMEMA were too soft to be manipulated, and were not suitable for 3D printing.

After establishing the resin, printing parameters optimization was carried out to achieve reliable 3D printing. One of the main challenges was to protect DNA from the well-known detrimental effects of prolonged UV exposure [30,31], therefore proper precautions have been implemented. Since UV-A is less harmful than UV-B [31], a printer with 385 nm light source was selected and the light dose finely modulated through the adjustment of the parameters, including time exposure and light intensity (Table S3, Supporting Information). To directly verify the biochemical integrity of the acrydite-DNA strands under these specific printing conditions, different electrophoretic runs were performed (Figure S1.b, Supporting Information). The analysis compared acrydite-DNAs exposed to a light dose that mimics the printing conditions, both in the presence and absence of photoinitiator, with not irradiated acrydite-DNA sequences. The results confirmed the absence of DNA fragments, demonstrating that the employed irradiation does not compromise the oligonucleotidic backbone. Furthermore, a shift toward higher molecular weight bands was observed in the presence of LAP. This is consistent with the radical polymerization of acrydite moieties, that lead to reaction products of higher molecular weight.

Still, the main goal was to maximize printing performance in terms of resolution, while limiting production time in a cost-effective manner. To this end, printing conditions were optimized to fabricate three samples in parallel using ultra-low resin volumes (< 100 µl). The printability of the resin strongly depends on the geometrical complexity of the target architecture. Simple solid geometries, such as cylinders (Fig. 2.a) and pyramids (Figure s5, Supporting Information), could be fabricated with good structural integrity and acceptable resolution. For these structures, the measured dimensions differed by approximately ± 200 µm along x and y directions and ± 50 µm along z from the corresponding CAD models for simple geometries like cylinders, a deviation that is reasonable considering that hydrogels with such amount of water have delayed gelation which limit the control of the polymerization propagation, and the process is sensitive to small variations in zero-levelling, particularly along the z direction. In contrast, objects featuring more complex geometrical details, such as internal cavities, sharp edges or thin walls, exhibited markedly reduced printing fidelity when fabricated using the transparent formulation. Representative examples include hollowed star-based prisms (Fig. 2.a) and a few other three-dimensional architectures reported in the Supporting Information (Figure S5, Supporting Information). In these cases, the high optical transparency of the resin led to insufficient confinement of the projected light, resulting in unintended polymerization beyond the designed layers and, consequently, poor definition of fine features. These observations highlight the intrinsic limitations of dye-free formulations for the fabrication of complex DNA-based hydrogel architectures and motivated the introduction of a light-absorbing dye to improve optical confinement during printing [32]. Based on these considerations, the resin formulation was further improved by incorporating a yellow dye, tartrazine, as light absorber, whose presence resulted in a clear improvement in printing resolution and reproducibility, enabling sharper features and more consistent dimensions, as illustrated by the yellow star-based prism in Fig. 2.a. In addition, Fig. 2.b shows more complex three-dimensional geometries obtained using the yellow resin. To further exploit the 3D printer potentialities and to assess DNA-specific response, a multi-material object has been printed, as shown in Fig. 2.c. The sample is made up of two co-axial cylinders with different diameters, the biggest one containing DNA and the smallest one without it, in the perspective of promoting the expansion of only the DNA-loaded part. Overall, the results are promising, showing the possibility to tune materials' properties in different layers. 3D printing seems effectively able to swiftly process DNA-based hydrogels with advanced geometries and well-designed composition through a versatile and maskless process.

After successful 3D printing, the mechanical behavior of the resins and the resulting hydrogels were investigated by means of (photo) rheological measurements, to assess the influence of DNA incorporation on material properties. Fig. 3 summarizes the rheological characterization performed on DNA-free and DNA-based systems. First, amplitude and frequency sweep tests were conducted on the liquid resin prior to photopolymerization (Fig. 3.a and 3.b). In this regime, both formulations exhibited comparable viscoelastic behavior, with no appreciable differences in storage (G') and loss (G'') moduli over the explored strain and frequency ranges. This indicates that the presence of DNA does not significantly alter the flow behavior or processability of the liquid resin and explains the reason why printing parameters are equal between the two formulations. The evolution of the viscoelastic properties during photopolymerization was then monitored by photorheological time-

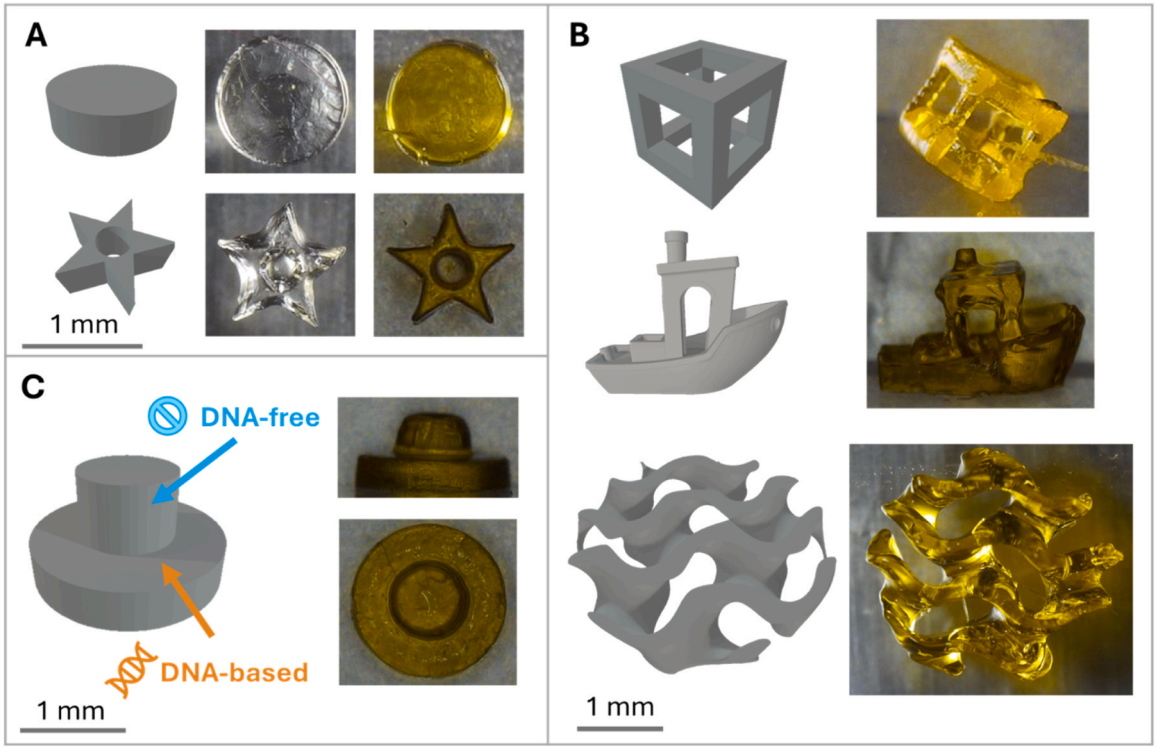

Fig. 2. 3D printing of DNA-based hydrogels by DLP. For all panels, the CAD model is shown on the left and the corresponding top view of printed hydrogels on the right. **a)** Comparison of simple geometries fabricated using dye-free (transparent) and tartrazine-containing resin formulations. **b)** Representative complex three-dimensional architectures printed using the tartrazine-containing formulation. **c)** Multi-material object consisting of two co-axial cylinders, printed using the transparent resin formulation, with the lower section containing DNA and the upper section being DNA-free.

sweep experiments (Fig. 3.c). Upon UV irradiation, both formulations showed a comparable transition period from a liquid-like to a solid-like response, followed by the characteristic increase of G′ and its eventual plateau. The similarity in the temporal evolution of G' indicates that the photopolymerization kinetics are essentially unaffected by the presence of DNA. Remarkably, the DNA-based resin exhibited a slightly higher plateau value of G' (about 6 kPa) compared to the DNA-free formulation (about 4 kPa), suggesting a modest increase in stiffness of the resulting network. This behavior can be indeed attributed to the presence of DNA molecules, which introduce additional crosslinking points within the hydrogel network due to the acrydite moieties (Fig. 1.c). Finally, amplitude sweep tests were performed on the fully photopolymerized hydrogels to evaluate their linear viscoelastic (LVE) region (Fig. 3.d). Both DNA-free and DNA-containing hydrogels displayed comparable LVE ranges, indicating similar resistance to deformation under small strains. While the DNA-free hydrogel exhibited a slightly extended LVE region, the overall mechanical response of the two systems remained largely comparable in the solid state too.

Afterwards, the hydrogels responsiveness to complementary DNA molecules was assessed. As previously mentioned, the triggering was controlled by immersing the hydrogels into a buffer containing nucleic acidic fuel, namely complementary hairpins. However, since swelling is an intrinsic property of hydrogels, it was crucial to distinguish this effect from the one induced by the DNA-triggered reaction. To do so, the experimental expansion protocol was designed in two sequential phases. First, the printed samples were immersed in TAE/Mg^{2+} for 48 h, an adequate time frame for the expansion to plateau. Then, the buffer was replaced by another one containing hairpins and samples were incubated for an additional 96 h to allow full progression of the process.

It is important to emphasize that the expansion induced by both TAE/Mg^{2+} and the HCR process is inherently volumetric. However, due to the softness of the hydrogel and the physical constraints of the measurement system, the variation in surface area was identified as the most robust and reproducible parameter for quantifying the expansion. To validate this approach, a detailed dimensional analysis was performed on the xy and xz planes (Figure S6, Supporting Information). The results indicate that the initial swelling in TAE/Mg^{2+} is slightly anisotropic, with the xy expansion being more pronounced than the growth along the z-axis. This effect can be possibly due to the DLP fabrication process, where the light attenuation through the resin layer can lead to a non-homogeneous crosslinking density [33]. The subsequent DNA-driven expansion phase was, instead isotropic, since the relative expansion rates for the xy and xz planes were identical. Based on these observations, solely the measurement of the xy surface area was adopted as a practical and sufficiently representative indicator for the overall expansion. While this approach does not directly capture the full volumetric displacement, the consistent expansion rates across the different axes allow for a reliable comparison between samples (Figure S7).

It should be also noted that, while tartrazine was introduced to improve printing fidelity, its presence during the DNA-triggered actuation experiments was intentionally avoided since the interaction of tartrazine with DNA and its potential genotoxicity have been the subject of debate in the literature [34–36]. In particular, the initial swelling step in TAE/Mg^{2+} served a dual purpose: allowing the hydrogel to reach its equilibrium swelling state and promoting the diffusion-driven removal of the dye from the polymer network. The effective washing-out of tartrazine during this phase was quantitatively monitored via UV–visible spectroscopy and supported by IR spectroscopy and visual color changes (Figure S8, Supporting Information). The analysis of the characteristic absorption peak of tartrazine (426 nm) showed a reduction of approximately 98% after the washing phase, confirming nearly complete removal from the polymeric network.

Once the dye was removed and the system reached equilibrium, the second phase of expansion was analyzed. Fig. 4.a illustrates the progression of hydrogels' surface area after each phase. To precisely control the DNA-driven expansion dynamics and prevent uncontrolled growth,

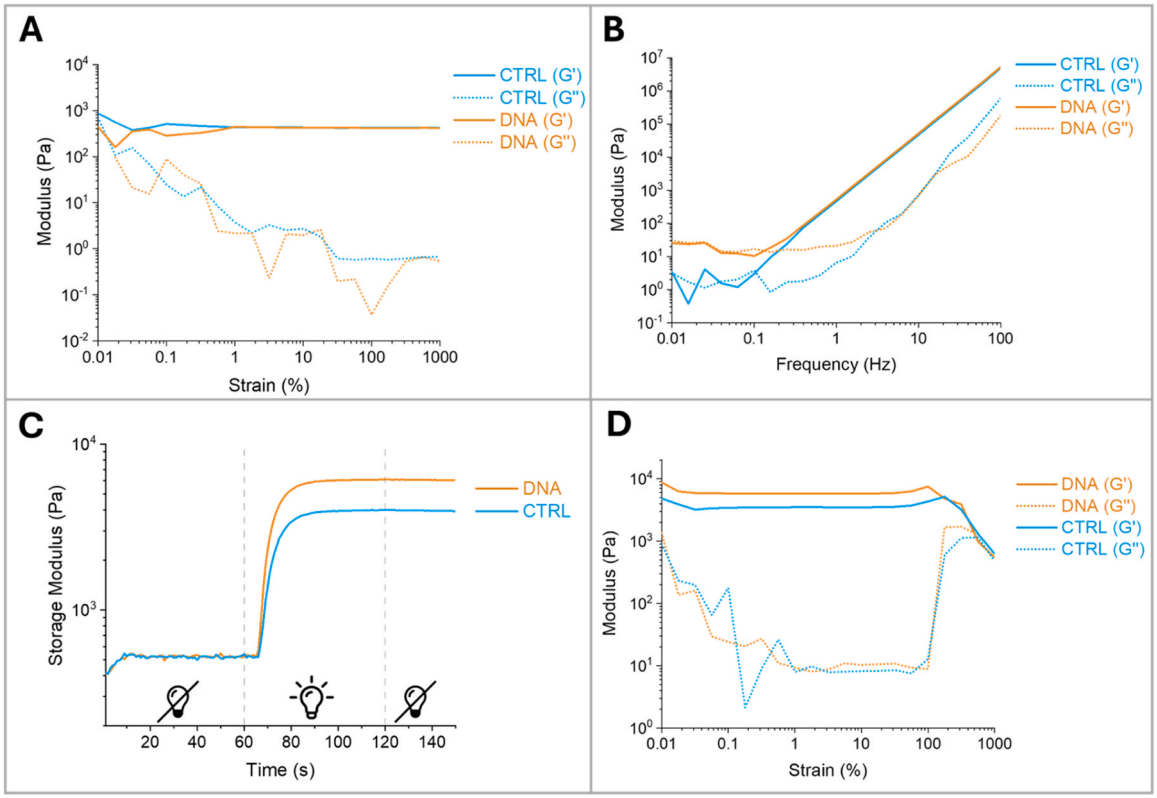

Fig. 3. (Photo)rheological characterization of DNA-free and DNA-based hydrogel formulations. **a)** Amplitude sweep and **b)** frequency sweep measurements performed on liquid resins prior to photopolymerization, showing the storage modulus (G′) and loss modulus (G″). **c)** Photorheological time sweep during UV irradiation (light source at 365 nm), reporting the evolution of the storage modulus during photopolymerization. Irradiation started after 60 s and ended after 120 s. **d)** Amplitude sweep performed on photopolymerized hydrogels to determine the linear viscoelastic (LVE) region, showing G′ and G″.

terminator hairpins ($H1_T$, $H2_T$) were added to the buffer containing standard complementary hairpins (H1, H2), as suggested by literature [16]. Under these conditions, the DNA-based hydrogels achieved a significant expansion of approximately 43% with respect to the swelled state and 190% with respect to the printed one. The specificity of this response was confirmed by two control experiments. The negative control consisted of immersing a DNA-free hydrogel within the expansion buffer, while the positive control was a DNA-based hydrogel exposed to a buffer containing non-complementary hairpins ($H1_C$, $H2_C$). Both controls didn't show further expansion with respect to the swelling dimensions, addressing the expansion exclusively to the sequence-specific hybridization. Note, the experiments reported are consistent with similar measurements performed on specimens produced without tartrazine (Figure S9).

The robustness of this DNA-related functionality was further explored by assessing its selectivity in more complex environments. When exposed to a blend of complementary and non-complementary sequences, the hydrogel maintained its molecular recognition capabilities, exhibiting an expansion profile identical to that observed in the presence of pure complementary hairpins. The hydrogel retained its sequence-specific affinity even in the presence of an off-target genomic DNA extract from mycoplasma. Indeed, in the presence of the solely mycoplasma DNA, hydrogel didn't expand, while in a blend with complementary hairpins, it still responded with a faint expansion. We believe that the genomic DNA hindered hairpins availability to the HCR process probably due to crowding effects since it has been observed in literature that hairpins can be stabilized, with slower opening [37–39].

These results are evident in the multi-materials hydrogel, as reported in Fig. 4.b. The two cylinders swell in a similar way during the incubation in TAE/Mg^{2+}, while only the part containing DNA molecules further expands in the second phase. This suggests that DLP 3D printing has great potential in the creation of sophisticated objects responding to very precise local stimuli. This successful preservation of localized responsiveness within the printed architecture demonstrates that DLP 3D printing can produce complex, multi-material architectures, where specific domains act as autonomous, sequence-specific biosensors, capable of translating molecular recognition into a programmed swelling response.

To further evaluate that the observed expansion was specifically induced by the DNA hairpins, we conducted additional experiments on the samples. Upon completion of the expansion process, both the DNA-based hydrogels and the control ones were washed and then immersed in a solution containing SYBR Safe (Fig. 5a). This exhibits fluorescence upon binding to DNA, allowing for the visualization of its presence [40].

After an overnight incubation period, during which SYBR Safe diffused throughout the hydrogels, fluorescence was recorded. As expected, DNA-free samples, i.e. the negative control, Fig. 5.b showed no fluorescence signal when immersed in TAE/Mg^{2+}. While, after the immersion in the expansion buffer (Fig. 5.c), an evident signal coming from the hydrogel surroundings appeared, suggesting the presence of residual DNA hairpins within. Conversely, in the case of DNA-based hydrogels (Fig. 5.d), the samples manifested a strong fluorescence while a faint intensity was visible in their surroundings. By comparing the control hydrogels and the DNA-based ones, the sequence-dictated migration of DNA hairpins toward the hydrogel core becomes evident. In the presence of DNA sequences within the hydrogel, indeed, hairpins are bonded to it, resulting in their depletion from the buffer and, thus, in the loss of the fluorescence signal. In contrast, this clearly doesn't happen in the control samples, where the absence of target molecules prevents any hairpin from being entrapped in the scaffold.

Therefore, we can reasonably assume that the further expansion observed only in the DNA-based hydrogels is due to the integration of

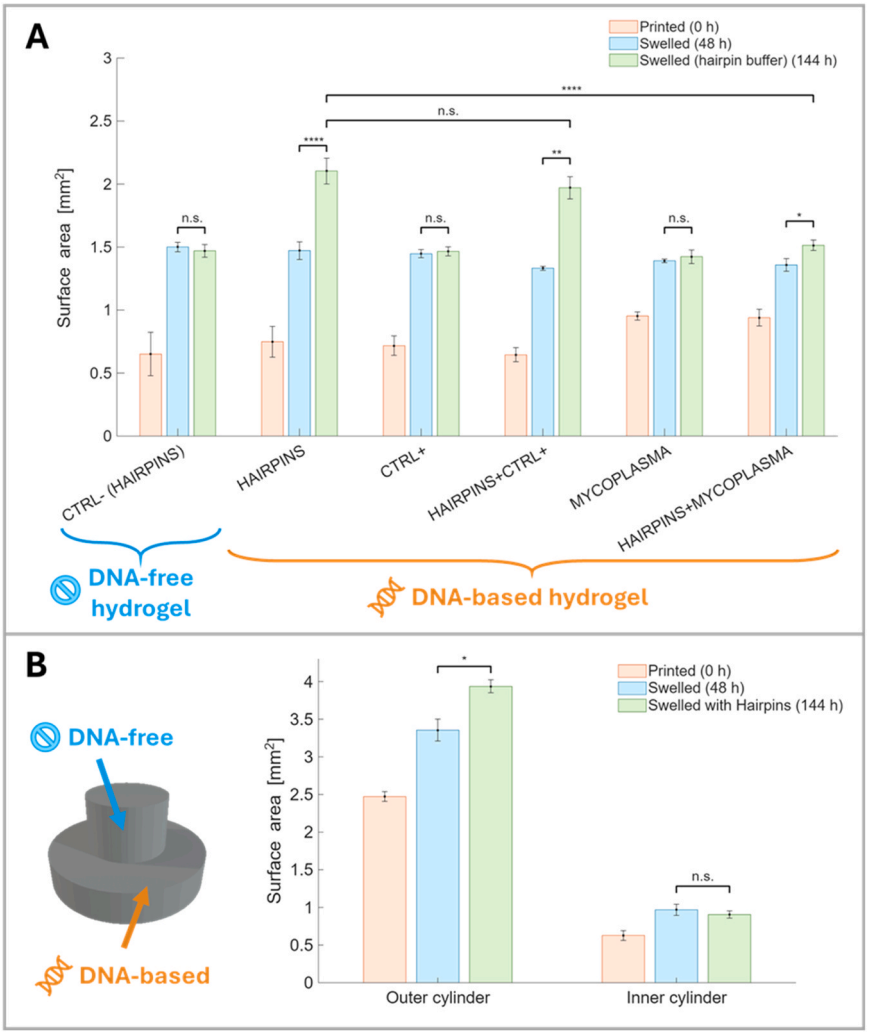

Fig. 4. a) Bar chart of the surface area variation of DNA-free and DNA-based hydrogels during the DNA-driven expansion process. DNA-free hydrogels have been exposed to complementary hairpins (H1,H1$_T$, H2, H2$_T$) while DNA-based hydrogels have been added to different DNA-containing buffers (from left: complementary hairpins, non-complementary hairpins, a blend of both, genomic DNA from mycoplasma, a blend of hairpins and genomic DNA. b) Bar chart of the surface area variation of a multi-material object. The surface variation of the outer cylinder (DNA-containing hydrogel) is compared with the one of the inner cylinder (DNA-free hydrogel). Orange bars correspond to the dimensions after printing (t = 0 h), blue bars to the equilibrium swelling in TAE/Mg^{2+} (t = 48 h) and green bars to the HCR-induced expansion in the presence of DNA molecules (t = 144 h). Error bars represent the standard deviation. * = $p < 0.05$, ** = $p < 0.01$, **** = $p < 0.0001$, 'n. s.' = $p > 0.05$.

hairpins within its internal structure and we can also confirm that the hydrogel preserved its functionality, regardless of the fabrication process. Those results are in good agreement with the previous results obtained by stereolithography.

To cross-check these data, FT-IR analysis was performed on lyophilized samples. A preliminary evaluation confirms the HCR-induced expansion from data reported in Fig. 6.a

The signals related to the polymeric part of the hydrogels were first assigned. Consistent with previous literature reports, the negative control showed characteristic peaks of both the PEG-derived (meth)acrylates as ether stretching at 1094 cm^{-1} , ester carbonyl at 1730 cm^{-1} and methylene vibrations at 2870 cm^{-1} [41–43]. These bands remained unchanged after the expansion phase, indicating that the polymer backbone is stable throughout the addition of DNA hairpins, highlighted by the essentially flat subtraction profile between the spectra before and after expansion (Fig. 6.b).

The DNA-based hydrogel before the DNA-driven expansion exhibited a spectrum that was overall very similar to the control one, suggesting that the DNA contribution was low compared to the polymer backbone and largely masked by its absorptions. However, a faint difference can be observed within the 1500–1700 cm^{-1} region, suggesting the presence of bands associated with nitrogenous bases. To confirm, the control spectrum was subtracted to the data obtained, revealing clear signals assigned to DNA (Fig. 6.c), such as the asymmetric stretching of the phosphate group at 1240 cm^{-1} and DNA backbone vibrations at 1050 and 967 cm^{-1}. These peaks reflect the dehydrated nature of our freeze-dried samples, matching the A-form of dsDNA, in good agreement with earlier literature studies [44,45].

Following the incubation with hairpins, the DNA hydrogel displayed a distinct spectrum compared with all the others exhibiting new peaks, indicating structural changes during the DNA-driven expansion. The nucleic acid component became prominent, with characteristic bands assignable to nitrogenous bases vibrations (1603 cm^{-1} for adenine with a shoulder at 1577 cm^{-1} corresponding to guanine, 1650 cm^{-1} for cytosine and 1698 cm^{-1} for thymine) [45]. Moreover, the increased intensity in the subtraction spectrum compared to the DNA hydrogel before expansion indicates, in a semi-quantitative way, a higher DNA content within the expanded hydrogel, thus confirming the success of the HCR process.

Having demonstrated not only the successful activation of the HCR

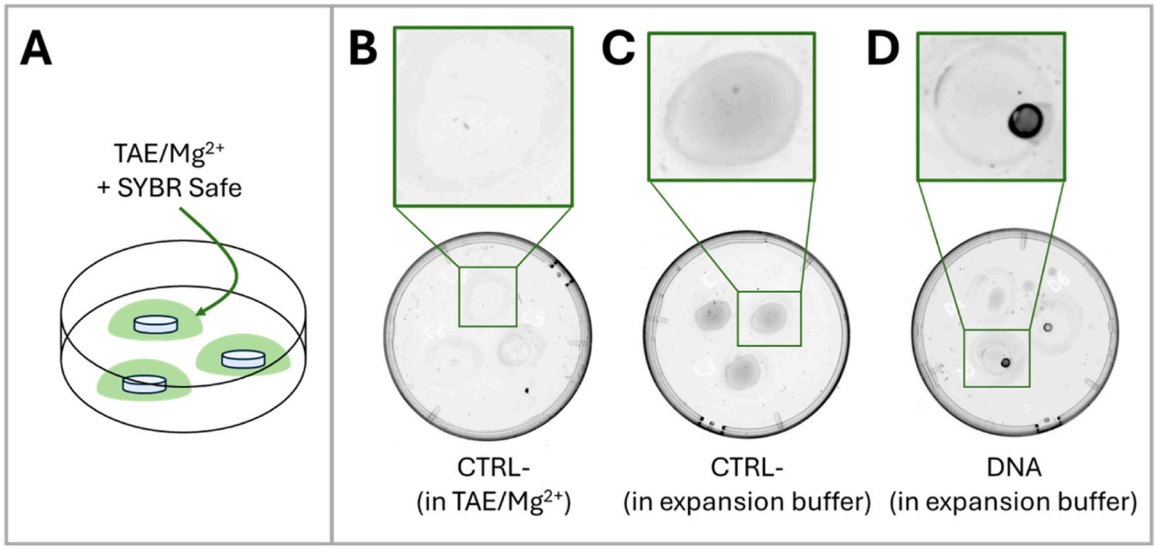

Fig. 5. a) Schematic illustration of the set-up for the fluorescence essay. b) Control hydrogels after incubation in TAE/Mg^{2+}. c) Control hydrogels after incubation in the expansion buffer. d) DNA-based hydrogels after incubation in the expansion buffer.

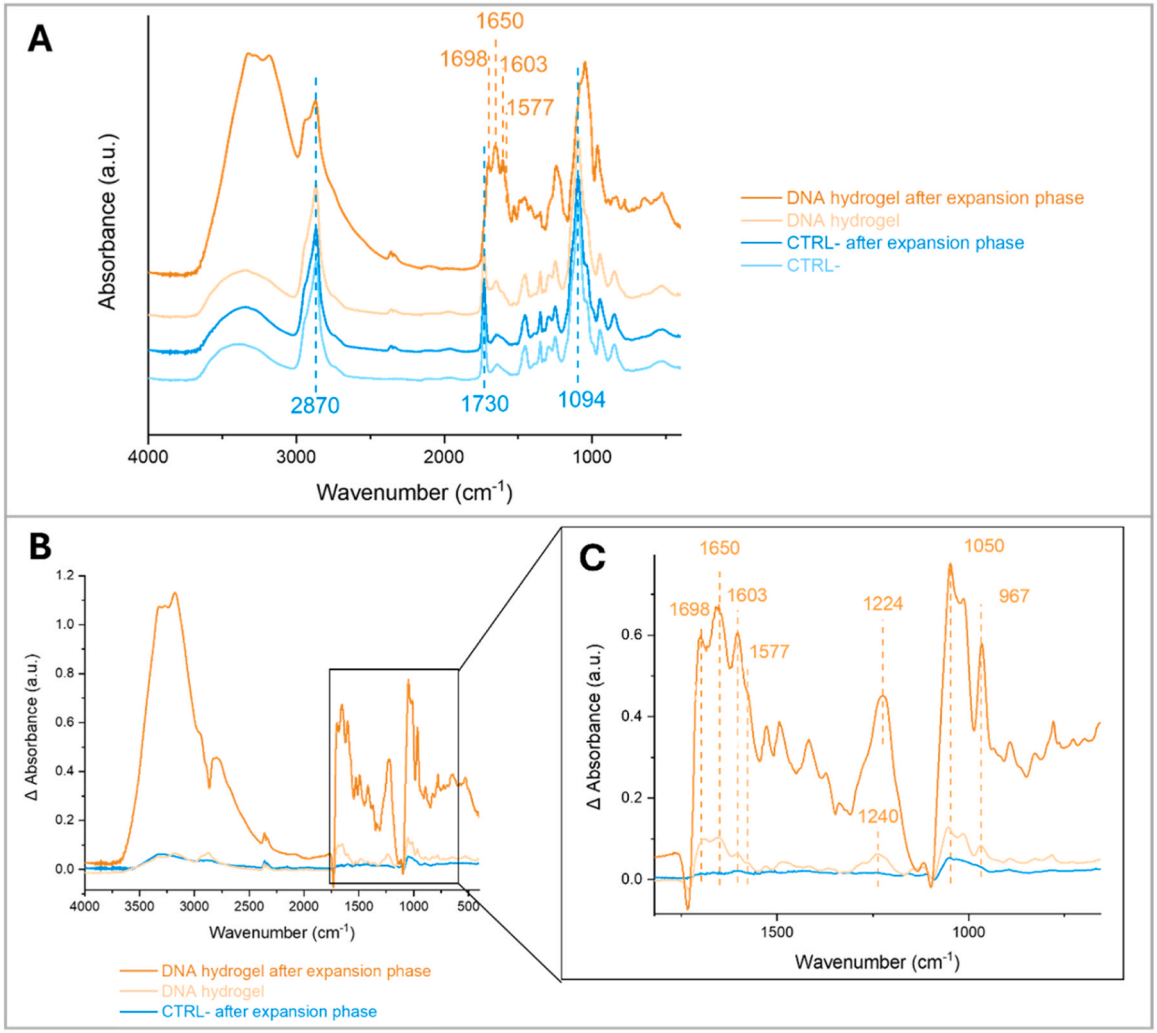

Fig. 6. a) FT-IR spectra of the negative control and DNA-based hydrogels recorded before and after HCR expansion phase. b) Difference FT-IR spectra obtained by subtracting CTRL- signal from the other spectra. c) Enlarged view of the 700–1700 cm^{-1} range.

process but also its sequence-dictated specificity, the ability to reversibly modulate the hydrogel dimensions was subsequently investigated. To

this end, an external thermal stimulus was employed to induce the dehybridization of the DNA duplexes formed during HCR.

Expanded hydrogels were subjected to a thermal treatment at 80 °C for 20 min under humid conditions and were then rapidly cooled to room temperature. This protocol promoted DNA dehybridization and favored intramolecular refolding of the hairpins upon cooling, enabling their dissociation from the acrydite-modified strands and diffusion out of the hydrogel matrix (Fig. 7.a). Following this treatment, the hydrogels exhibited a marked reduction in size, approaching the dimensions measured after the initial swelling step, as shown in Fig. 7.b and Figure S10. Dimensional recovery occurred without macroscopic damage to the structures, indicating that the polymer network remained intact.

The cycle of HCR-induced expansion and thermally induced contraction can be repeated multiple times. As a proof of concept, two consecutive cycles were successfully performed, highlighting the reusability of the system. In contrast, negative control samples exposed to the same thermal treatment did not display any appreciable dimensional change, confirming that the observed reversibility originates from DNA-mediated interactions rather than from the hydrogel matrix itself.

Additional confirmation of hairpin release was obtained by IR spectroscopy, as illustrated in Fig. 7.c-e. Differential spectra, obtained by subtracting the signal of the control hydrogel, showed that after thermal contraction the spectral features associated with the HCR-expanded state were significantly reduced, yielding a profile closer in amplitude to that of the swollen pre-HCR hydrogel. This semi-quantitative observation is consistent with the effective removal of the hybridized hairpins from the network, further corroborating the reversible and DNA-driven nature of the actuation mechanism.

4. Conclusion

This study has investigated a new process to fabricate functional DNA-based hydrogels. Specifically, we have taken advantage of the vat DLP 3D printing technology which, compared to other conventional light-based methods, brings the hydrogel structure to the third dimension. Thus, inspired by previous works based on photolithographic processes, photocurable DNA-based resins were synthesized, progressively optimized in terms of composition and optical properties, and finally applied to 3D printing process. In particular, the addition of a light-absorbing dye enabled a significant improvement in printing resolution and fidelity, allowing the fabrication of more complex three-dimensional architectures. The hydrogel functionality was also investigated by the addition of complementary DNA hairpins, through the hybridization chain reaction process, whose outcome resulted in the volumetric increase of the samples. The DNA-triggered response was shown to be highly specific, as no dimensional changes were observed in the presence of non-complementary control sequences. Additional experiments confirmed the selectivity of the hydrogel and the robustness of the system, as the volumetric expansion was successfully triggered even with a mixture of complementary and non-complementary DNA sequences. In particular, it maintained its functional response even in the presence of longer DNA sequences that would typically hinder the HCR reaction in less optimized systems, due to not specific interactions or steric interference.

The 3D printed hydrogels fabricated show complex geometries, good

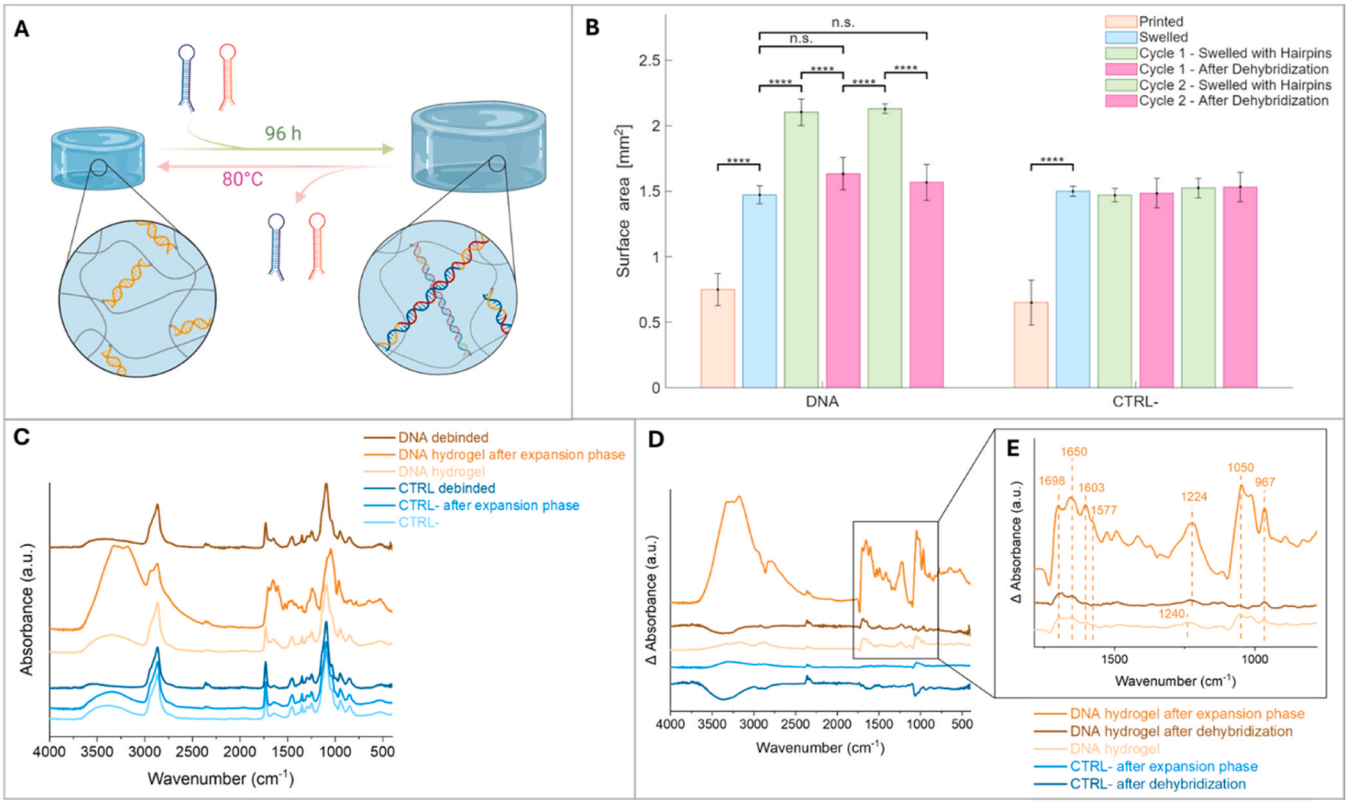

Fig. 7. a) Schematic illustration of the dehybridization process of DNA-based hydrogels. b) Bar chart of the surface area variation of DNA-based hydrogels and control samples during two consecutive cycles of DNA-driven expansion and thermal contraction. Orange bars correspond to the dimensions after printing, blue bars to the equilibrium swelling in TAE/Mg^{2+}, green bars to the HCR-induced expansion in the presence of complementary hairpins and magenta bars to the dimensions measured after thermal treatment, corresponding to DNA dehybridization and hydrogel contraction. The second expansion–contraction cycle follows the same sequence of steps and, thus, the same colors. Error bars represent the standard deviation. **** = $p < 0.0001$, 'n.s.' = $p > 0.05$. c) FT-IR spectra of the negative control and DNA-based hydrogels recorded before, after HCR expansion phase and after the thermal dehybridization phase. d) Difference FT-IR spectra obtained by subtracting CTRL- signal from the other spectra. e) Enlarged view of the 700–1700 cm^{-1} range.

resolution and CAD fidelity. Additionally, multi-material structures were successfully fabricated, showing the possibility to control the composition layer by layer. Mechanical characterization further demonstrated that the incorporation of DNA leads to moderate increase in the stiffness of the hydrogels, without affecting the printability of the resin. The specimens produced were able to expand up to 190% of their initial dimensions. This implies that DLP 3D printing does not spoil the hydrogel functionality, also confirmed by electrophoretic runs, and therefore this technology can be a straightforward alternative to photolithography to fabricate DNA responsive hydrogels. Finally, the effective inclusion of DNA was also demonstrated by fluorescence essay, which showed clear signals only in the samples that were expanded by DNA strands. Importantly, it was demonstrated that the HCR-driven expansion was reversible: a thermal treatment induced DNA dehybridization, allowing the hydrogels to recover dimensions close to their initial state and enabling repeated actuation cycles.

This study represents a further evolution for DNA-based technologies. On the other hand, despite the several advantages of this process in terms of cost-effectiveness and fabrication velocity illustrated, it represents just the first step for future applications, which will require synergic development, both in terms of materials and design. Such advancements would facilitate the development of devices suitable for a wide range of applications, in particular advanced biosensing, as demonstrated in this work. However, other applications fields can be explored, such as soft robotics and targeted drug delivery systems, where the structure design can become crucial.

5. Experimental section

5.1. Materials

Polyethylene glycol diacrylate (PEGDA, 700 Da) and polyethylene glycol methyl ether methacrylate (PEGMEMA, 950 Da) have been selected as pre-polymers for the hydrogel bulk. Lithium phenyl-2,4,6 trimethylbenzoylphosphinate (LAP) has been chosen as photoinitiator, after a comparison with TPO nanoparticles (TPO-SDS) and Irgacure 2959 (I2959). As light absorber, the yellow dye tartrazine has been added to the photocurable resins. These were all purchased from Merck. The choice of eight sequences of oligonucleotides (Table S1, Supporting Information) was inspired by Gracias et al.'s work.[16] C and C' strands were purchased from Integrated DNA Technologies with the 5' acrydite modification (a methacrylic phosphoramidite) to ensure their covalent integration within the hydrogel network during the 3D printing process. All the others DNA strands were purchased from Integrated DNA Technologies. Magnesium chloride ($MgCl_2$) has been dissolved in tris acetate-EDTA buffer (TAE) to obtain the final solution (TAE/Mg^{2+}), used as solvent for both the hydrogel resin and the expansion buffer. TAE was lab-synthesized from ethylenediaminetetraacetic acid (EDTA), glacial acid and tris-base. These ingredients and $MgCl_2$ were purchased from Merck. It was paid attention to the use of nuclease-free distilled water ($H2O^{N-}$) in substitution for the deionized one since the latter can be contaminated by exogenous DNases able to degrade nucleic acids, possibly decreasing the efficacy of the HCR process. For the electrophoretic runs of the DNA strands, a gel has been prepared with TAE and agarose (from Merck) and DNA has been stained with SYBR Safe (from Thermo Fisher Scientific). The latter has been employed for fluorescence analysis too.

5.2. Solvent preparation

TAE 50x was prepared following a common protocol [46]. Firstly, EDTA was dissolved in $H2O^{N-}$ to reach a concentration of 0.5 M and pH was adjusted to 8 by the addition of NaOH. Then, tris-base was dissolved in $H2O^{N-}$ and, when the solution appeared homogeneous, glacial acid and the EDTA solution previously prepared were slowly added. TAE was ready after the dilution to 2X. $MgCl_2$ powder was dissolved in $H2O^{N-}$ to obtain a concentration of 25 mM. The final solvent (TAE/Mg^{2+}) was completed after blending 1:1 of TAE 2X and 25 mM $MgCl_2$.

5.3. DNA preparation

All the DNA strands were received in a lyophilized form and, subsequently, suspended in TAE/Mg^{2+} with a concentration of 2 mM for each strand of the expansion buffer (H1, H2, $H1_T$, $H2_T$, $H1_C$, $H2_C$) and 25 mM for the strands belonging to the photocurable resin (C and C'). Then, each strand singularly underwent a thermal cycle with Bio-Rad C1000 Touch PCR Gradient Thermal Cycler, except for the C and C' strands. Before the exposure to temperature, these were firstly resuspended in a common solution (3 mM) in order to hybridize. Temperature was set at 90°C and then lowered to 20°C in a quasi-static way: the velocity rate was –0,1 °C s-1 and for each variation of 10°C the temperature remained constant for 30 s. Gel electrophoresis tests were performed to verify, firstly, the C-C′ hybridization and, secondly, to confirm that their molecular integrity was preserved after UV exposure. Agarose (at 1% w/v and 4% w/v respectively for the two experiments) was dissolved in TAE 1X for 30 s in a microwave at the highest power level, then SYBR Safe was added in 1:10,000 proportions and the gel was let jellify in an appropriate mold. For the second experiment, C-C′ strands were exposed to 385 nm UV light at a dose of 30 mW cm-2 for 10 s (both with and without the presence of the LAP photoinitiator) to simulate the conditions occurring during the 3D printing process. Electrophoretic results are available in Figure S1, Supporting Information.

5.4. Mycoplasma DNA amplification

For mycoplasma DNA amplification from contaminated cell culture medium, a previously described protocol was used [47]. Specifically, a direct PCR method targeting a highly conserved region within the 16S rRNA gene was performed. The reaction utilizes a specific sense primer GPO-3 (5′-GGGAGCAAACAGGATTAGATACCCT-3′) and the antisense primer MGSO (5′-TGCACCATCTGTCACTCTGTTAACCTTC-3′) both purchased from Integrated DNA Technologies. For the amplification reaction, the KAPA Taq HotStart with dNTPs kit (Roche) was used following manufacturer protocols. The resulting amplicon length is 270 bp.

5.5. Resin preparation

The hydrogel formulation consisted of 10% wt pre-polymers, 0.2% wt LAP, 1.154 mM hybridized C-C' DNA and TAE/Mg^{2+}. Starting from a resin only based on PEGDA, different proportions of PEGMEMA were added. Rheological tests directed the choice toward the 2:1 molar ratio of, respectively, PEGDA and PEGMEMA. All the ingredients have been mixed up together and, subsequently, vortexed until the formulation appeared clear. A control formulation (CTRL-), non-containing DNA strands, was prepared in analogy. In the case of the yellow formulations, either CTRL- or DNA-based, 0.1% wt tartrazine has been added to the aforementioned components to improve the 3D printing resolution.

5.6. UV–visible spectroscopy

The absorbance spectra of the PEGDA-based formulations containing three different photoinitiators (LAP, TPO-SDS and I2959) and the absorbance spectra of the hydrogels containing tartrazine have been obtained by means of the BioTek Synergy HTX Multi-Mode microplate reader. Absorbance tests have been performed between 300 nm and 750 nm with intervals of 1 nm.

5.7. Rheological tests

Rheological and photorheological tests have been performed on PEGDA-based resins containing different photoinitiators, on resins with different ratios of PEGDA and PEGMEMA and on final DNA-loaded

resins by means of a rheometer Anton Paar MCR 302 with plate-plate configuration. For the first two experimental sets (screening of the photoinitiator and comparison of different PEGDA-PEGMEMA ratios), plates of 25 mm were used, whereas 5 mm plates were used for the third one (actual characterization of DNA-containing resins) because of the limited availability of the DNA resin. For all tests, temperature was set at 25°C and plate-plate distance at 200 μm. During the shear rate test, in which the viscosity variation has been evaluated, the shear rate has been varied in the range between 1 and 1000 s^{-1}.

During the time sweep test, which shows the material behavior when irradiated by UV light, strain was set at 1% and frequency at 1 Hz. The protocol followed during this last consists in measuring the storage modulus G' of the resin during the entire process of photopolymerization. For the first two experiments, the mechanical behavior of the liquid resin was evaluated was evaluated for 30 s, then samples were irradiated with UV light for 150 s until G' steadily plateaued, eventually the test ended after an additional 20 s to evaluate the properties of the solid sample. In analogy, for the third experiment the protocol was slightly adjusted as follows: evaluation of G' of the liquid resin for 60 s, UV-light irradiation for other 60 s and evaluation of G' of the solid sample for 30 s. The UV Hamamatsu LC8 wide-spectrum lamp (365 nm) was the light source employed for photopolymerization. To complement the mechanical characterization of the liquid resins, an amplitude sweep test (with frequency at 1 Hz and strain varied from 0.01% to 1000%) and a frequency sweep test (with strain at 1% and frequency varied from 0.01 to 100 Hz) were accomplished. An amplitude sweep test with same parameters was also performed on photopolymerized samples to estimate the LVE region.

All the tests are available in Fig. 3 and Figure S2 and S4, Supporting Information.

5.8. 3D printing

During the fabrication process, the final custom-made resins have been photopolymerized by a DLP 3D printer (Asiga Max X27 UV), with LED light source that can generate 385 nm UV light. The desired geometries, shown in Fig. 2, have been designed on SolidWorks and CADs have been exported to.STL format to match the printer software (Asiga Composer) requirements, except from the "benchy boat" CAD whose file.STL has been imported from an open-source repository. To avoid resin wastage and DNA prolonged contact with UV light, only 15 μL of formulation at a time have been charged into the vat to produce up to three samples in parallel. Good printability has been reached by setting the layer thickness to 15 μm, light intensity to 23 mW cm^{-2} and the exposure time to 8 s for burn-in, 6 s for all the other layers (Table S3, Supporting Information). Some other marginal parameters, such as the platform approach and separation velocity, have been adjusted according to the CAD. During the post-curing phase, the exceeding liquid formulation was recovered and set aside to be re-used later, while the hydrogel was gently tapped with absorbent paper to remove any further non-polymerized residues.

5.9. DNA-driven swelling protocol

Once hydrogels have been printed, their ability to expand in a buffer containing complementary DNA strands has been tried out. The expansion buffer was made up of H1 and H2 hairpin, to whom terminator hairpins ($H1_T$ and $H2_T$) have been added to better control the HCR process [16]. Each type of hairpin has been suspended in TAE/Mg^{2+} at the concentration of 40 μM, consisting of 98% of normal polymerizing ones and 2% of terminal ones. Once added all the strands to the solvent, the solution was vortexed until it appeared clear. As control (CTRL+), an expansion buffer containing 40 μM of each non-complementary DNA hairpin ($H1_C$ and $H2_C$) has been produced in an analogous manner. The expansion protocol has been divided into two steps: first, hydrogels were left swelling in TAE/Mg^{2+} at room temperature for 48 h until they reached saturation, then the buffer was replaced by the proper DNA-based one for 96 h at room temperature to let the hairpins reach the hydrogel bulk and perform the HCR process. Each sample has been immerged in 25 μL of buffer in a controlled environment to avoid the solvent evaporation. This specific volume was calculated to maintain a precise 3:1 molar ratio between the hairpins (H1, $H1_T$, H2, $H2_T$) and the acrydite-DNA strands and, thus, to ensure a sufficient stoichiometric excess to drive the HCR-mediated expansion to completion.

5.10. Thermally-induced dehybridization protocol

To induce DNA dehybridization and reverse the HCR-driven expansion, expanded hydrogels were subjected to a thermal treatment. Each sample was placed in 40 μL of nuclease-free distilled water to maintain a humid environment and prevent dehydration during heating. Then, they were heated at 80°C for 20 min using a Memmert VO200 oven.

Immediately after the thermal treatment, the samples were rapidly removed from the heating device and exposed to ambient conditions. This step was designed to favor intramolecular refolding of the DNA hairpins over intermolecular hybridization, thereby promoting their dissociation from the Acrydite-DNA strands (C-C') within the hydrogel network and enabling diffusion out of the matrix.

The cycle composed of DNA-driven swelling and thermally-induced dehybridization could be performed multiple times by repeating the same steps.

5.11. Fluorescence analysis

After completion of the expansion process, the buffer was substituted by one containing SYBR Safe in 1:10,000 dilution. As solvent, TAE x1 was used. Hydrogel samples have been incubated overnight in 25 μL of the staining solution, then ChemiDoc Imaging System (BIO-RAD) has been employed to get the images.

5.12. FT-IR spectroscopy

Samples were freeze-dried for 5 days in order to conduct Fourier Transform Infrared (FT-IR) spectroscopy. Thermo Fisher Scientific Nicolet Apex Spectrometer was used in the range of 4000 – 400 cm^{-1} in attenuated total reflectance (ATR) mode with a diamond crystal. All spectra were recorded at a resolution of 4 cm^{-1} , averaging 64 scans per spectrum. Spectra were baseline-corrected and normalized to the polymer backbone peak at 1094 cm^{-1} . Difference spectra were obtained by subtracting the control hydrogel spectrum from the others.

5.13. Quantification of dimensional changes

A digital microscope (Andonstar ADSM301) has been employed to capture pictures of the samples top section at each timepoint, aiming to quantify the size variation in geometrical terms. The objective-sample distance was kept constant at 5.75 cm during all the measurements at the maximum magnification. Image Processing MATLAB tools helped to count the number of pixels corresponding to the surface area of the hydrogel. Specifically, a region of interest (ROI) was manually identified thanks to Image Segmenter and converted into a binary file, while Image Region Analyzer returned data about the ROI area as number of pixels. ImageJ was used to identify the correspondence between the number of pixels and millimeters, so that the area could be expressed in mm^2. Due to the instrumental limitations, the (de)swelling ratio has only been identified with the surface variation and not in volumetric terms. Thus, considering the sample at the current timepoint (S_s) and the sample after printing (S_i), the percentual surface area has been defined as:

$$\textbf{Percentual Surface Area}_{\%} = \frac{\mathbf{S_s}}{\mathbf{S_i}} \cdot \mathbf{100} \quad (1)$$

Statistical analysis: Statistical elaboration has been performed over at

least six replicates and statistical tests supported the significance of the outcomes. To assess the normality of data coming from the replicates, the Shapiro-Wilk's test was picked up because of the limited dataset available and its null hypothesis consisted in declaring the normality of data [48]. Then, the paired Student test (paired T-test) was chosen, once all its assumptions were verified, to determine whether samples grew over time or not. If hydrogels swell, the surface mean value should be different at two different timepoints. The null hypothesis consisted in assessing the non-expansion of samples. To compare the dimensions of two different samples at the same time point, the two-sample Student test (two-sample *t*-test) has been used. The null hypothesis consisted in assessing the same surface area. For all tests, confidence interval was set at 95% and the null hypothesis was rejected for p-values less than 0.05. An open-source algorithm has been used for the Shapiro-Wilk's test [49], while the Student tests were picked from Statistics and Machine Learning Toolbox (MATLAB).

CRediT authorship contribution statement

Désirée Baruffaldi: Writing – review & editing, Investigation. **Candido Fabrizio Pirri:** Writing – review & editing, Funding acquisition. **Cristiana Drago:** Writing – original draft, Investigation. **Ignazio Roppolo:** Writing – original draft, Supervision, Conceptualization. **Francesca Frascella:** Writing – review & editing, Supervision, Methodology.

Declaration of Competing Interest

The authors declare the following financial interests/personal relationships which may be considered as potential competing interests: This work was supported by the National Plan for Complementary Investments to the NRRP, project "D34H—Digital Driven Diagnostics, prognostics and therapeutics for sustainable Health care" (project code: PNC0000001), Spoke 4 funded by the Italian Ministry of University and Research. If there are other authors, they declare that they have no known competing financial interests or personal relationships that could have appeared to influence the work reported in this paper.

Acknowledgments

This work was supported by the National Plan for Complementary Investments to the NRRP, project "D34H—Digital Driven Diagnostics, prognostics and therapeutics for sustainable Health care" (project code: PNC0000001), Spoke 4 funded by the Italian Ministry of University and Research.

Appendix A. Supporting information

Supplementary data associated with this article can be found in the online version at doi:10.1016/j.addma.2026.105231.

Data availability

Data will be made available on request.

References

[1] A. López-Díaz, A.S. Vázquez, E. Vázquez, Hydrogels in soft robotics: past, present, and future, ACS Nano 18 (2024) 20817–20826.
[2] P. Sikdar, et al., Recent advances in the synthesis of smart hydrogels, Mater. Adv. 2 (2021) 4532–4573.
[3] M. Neumann, et al., Stimuli-responsive hydrogels: the dynamic smart biomaterials of tomorrow, Macromolecules 56 (2023) 8377–8392.
[4] I. Roppolo, M. Caprioli, C.F. Pirri, S. Magdassi, 3D printing of self-healing materials, Adv. Mater. 36 (2024) 2305537.
[5] Z.M. Png, et al., Stimuli-responsive structure–property switchable polymer materials, Mol. Syst. Des. Eng. 8 (2023) 1097–1129.
[6] N.C. Seeman, H.F. Sleiman, DNA nanotechnology, Nat. Rev. Mater. 3 (2017).
[7] S. Bayda, M. Adeel, T. Tuccinardi, M. Cordani, F. Rizzolio, The history of nanoscience and nanotechnology: from chemical–physical applications to nanomedicine, Molecules 25 (2020).
[8] S. Nagahara, T. Matsuda, Hydrogel formation via hybridization of oligonucleotides derivatized in water-soluble vinyl polymers, Polym. Gels Netw. 4 (1996) 111–127.
[9] M. Chen, et al., Stimuli-responsive DNA-based hydrogels for biosensing applications, J. Nanobiotechnol. 20 (2022) 40.
[10] S. Kahn, J. Hu, Y, I. Willner, Stimuli-responsive DNA-based hydrogels: from basic principles to applications, Acc. Chem. Res. 50 (2017) 680–690.
[11] J. Shi, Z. Shi, Y. Dong, F. Wu, D. Liu, Responsive DNA-based supramolecular hydrogels, ACS Appl. Bio Mater. 3 (2020) 2827–2837.
[12] Q. Zhu, et al., Intelligent DNA-based hydrogels for bioanalysis and therapeutics, ACS Appl. Polym. Mater. 5 (2023) 6695–6719.
[13] W. Guo, et al., pH-stimulated DNA hydrogels exhibiting shape-memory properties, Adv. Mater. 27 (2015) 73–78.
[14] Y. Xing, et al., Self-assembled DNA hydrogels with designable thermal and enzymatic responsiveness, Adv. Mater. 23 (2011) 1117–1121.
[15] H. Kang, et al., Photoresponsive DNA-cross-linked hydrogels for controllable release and cancer therapy, Langmuir 27 (2011) 399–408.
[16] A. Cangialosi, et al., DNA sequence–directed shape change of photopatterned hydrogels via high-degree swelling, Science 357 (2017) *1979*.
[17] I. Kopyeva, R.P. Brady, C.A. DeForest, Light-based fabrication and 4D customization of hydrogel biomaterials, https://doi.org/10.1038/s44222-024-00234-w, Nat. Rev. Bioeng. (2024), https://doi.org/10.1038/s44222-024-00234-w.
[18] R. Shi, et al., Multicomponent DNA polymerization motor gels, Small 16 (2020).
[19] R. Shi, et al., Programming gel automata shapes using DNA instructions, Nat. Commun. 15 (2024) 1–11.
[20] Y. Kasahara, Y. Sato, M.K. Masukawa, Y. Okuda, M. Takinoue, Photolithographic shape control of DNA hydrogels by photo-activated self-assembly of DNA nanostructures, APL Bioeng. 4 (2020) 16109.
[21] L. Bai, M. Li, J. Su, A perspective on light-based bioprinting of DNA hydrogels for advanced bone regeneration: implication for bone organoids, Int. J. Bioprint. 9 (2022) 432–437.
[22] M. Caprioli, et al., 3D-printed self-healing hydrogels via digital light processing, Nat. Commun. 12 (2021) 2462.
[23] A. Salas, M. Zanatta, V. Sans, I. Roppolo, Chemistry in light-induced 3D printing, ChemTexts 9 (2023) 4.
[24] P. Xiao, J. Zhang, 3D Printing with Light, De Gruyter, 2021, https://doi.org/10.1515/9783110570588.
[25] R.M. Dirks, N.A. Pierce, Triggered amplification by hybridization chain reaction, Proc. Natl. Acad. Sci. USA 101 (2004) 15275–15278.
[26] S. Bi, S. Yue, S. Zhang, Hybridization chain reaction: a versatile molecular tool for biosensing, bioimaging, and biomedicine, Chem. Soc. Rev. 46 (2017) 4281–4298.
[27] F. Wajdi, A.E. Tontowi, 3D printed stent from graphene-polyethylene glycol diacrylate using digital light processing technique, Manag. Syst. Prod. Eng. 32 (2024) 555–562.
[28] J.R. Choi, K.W. Yong, J.Y. Choi, A.C. Cowie, Recent advances in photo-crosslinkable hydrogels for biomedical applications, Biotechniques 66 (2019) 40–53.
[29] J.A. Beamish, J. Zhu, K. Kottke-Marchant, R.E. Marchant, The effects of monoacrylated poly(ethylene glycol) on the properties of poly(ethylene glycol) diacrylate hydrogels used for tissue engineering, J. Biomed. Mater. Res. 92A (2009) 441–450.
[30] R.P. Sinha, D.-P. Häder, UV-induced DNA damage and repair: a review, Photochem. Photobiol. Sci. 1 (2002) 225–236.
[31] M. Kciuk, B. Marciniak, M. Mojzych, R. Kontek, Focus on UV-induced DNA damage and repair—disease relevance and protective strategies, Int. J. Mol. Sci. 21 (2020).
[32] M. Gastaldi, et al., Functional dyes in polymeric 3D printing: applications and perspectives, ACS Mater. Lett. 3 (2021) 1–17.
[33] M. Hakim Khalili, et al., Mechanical behavior of 3D printed poly(ethylene glycol) diacrylate hydrogels in hydrated conditions investigated using atomic force microscopy, ACS Appl. Polym. Mater. 5 (2023) 3034–3042.
[34] S. Arsenault-Escobar, et al., Unveiling the tartrazine binding mode with ds–DNA by UV–visible spectroscopy, electrochemical, and QM/MM methods, Spectrochim. Acta A Mol. Biomol. Spectrosc. 292 (2023) 122400.
[35] M. Nassar, Cytological and chromosomal damages induced by tartrazine and two classes (III and IV) of caramel food dyes, Eur. J. Biol. Res. 12 (2022).
[36] P. Mpountoukas, et al., Cytogenetic evaluation and DNA interaction studies of the food colorants amaranth, erythrosine and tartrazine, Food Chem. Toxicol. 48 (2010) 2934–2944.
[37] S. Nakano, H. Karimata, T. Ohmichi, J. Kawakami, N. Sugimoto, The effect of molecular crowding with nucleotide length and cosolute structure on DNA duplex stability, J. Am. Chem. Soc. 126 (2004) 14330–14331.
[38] D. Collette, D. Dunlap, L. Finzi, Macromolecular crowding and DNA: bridging the gap between in vitro and in vivo, Int. J. Mol. Sci. 24 (2023).
[39] O. Stiehl, K. Weidner-Hertrampf, M. Weiss, Corrigendum: kinetics of conformational fluctuations in DNA hairpin-loops in crowded fluids (2013, N. J. Phys. 18 (2016) 099501 (15 113010). N. J. Phys.).
[40] P. Oatey, Imaging fluorescently stained DNA with CCD technology how to increase sensitivity and reduce integration times, Biotechniques 42 (2007) 376–377.
[41] Imani, M. & Sharifi, S.Monitoring of polyethylene glycol-diacrylate-based hydrogel formation by real time NMR spectroscopy2014.
[42] A. Alafnan, et al., Development and characterization of PEGDA microneedles for localized drug delivery of gemcitabine to treat inflammatory breast cancer, Materials 15 (2022).

[43] Taormina, G. Design and characterisation of polymeric nanocomposites for automotive sector by additive manufacturing technology2020. doi:10.13140/RG.2.2.11170.58562.
[44] E. Hettiarachchi, V.H. Grassian, Impact of surface adsorption on DNA structure and stability: implications for environmental DNA interactions with iron oxide surfaces, Langmuir 40 (2024) 27194–27205.
[45] M. Banyay, M. Sarkar, A. Gräslund, A library of IR bands of nucleic acids in solution, Biophys. Chem. 104 (2003) 477–488.
[46] Behle, A. & Pawlowski, A. Recipe for 50x TAE buffer. Preprint at https://doi.org/https://dx.doi.org/10.17504/protocols.io.gtvbwn6.
[47] L. Young, J. Sung, G. Stacey, J.R. Masters, Detection of mycoplasma in cell cultures, Nat. Protoc. 5 (2010) 929–934.
[48] A.R. Henderson, Testing experimental data for univariate normality, Clin. Chim. Acta 366 (2006) 112–129.
[49] Gardner-O'Kearny, W. Shapiro-Wilk/Shapiro-Francia Tests. ⟨https://it.mathworks.com/matlabcentral/fileexchange/88778-swft-shapiro-wilk-shapiro-francia-tests⟩2021.